Combustion Synthesis in the Ti-C-Ni-Mo System: Part I. Micromechanisms

J.C. LaSALVIA, D.K. KIM, R.A. LIPSETT, and M.A. MEYERS

Combustion-wave arresting experiments were conducted on Ti-C-Ni and Ti-C-Ni-Mo powder mixtures. The reactant powder mixtures were placed within a conical hole machined in a Cu block. The reaction was initiated at the base of the cone and proceeded down the cone axis, toward the apex, until the heat loss to the Cu block was sufficient to arrest the reaction. This enabled the postreaction characterization of the three distinct regions of the combustion wave: unreacted, partially reacted, and fully reacted. The unreacted region is characterized by removal of a surface scale on the Ti particles and Ti $\alpha \rightarrow \beta$ solid-state phase transformation. The partially reacted region is characterized by a number of physical processes and a distinct interface with the unreacted region. These processes include the formation of Ti-Ni phases, Ti-Ni melt, TiC_x layer on the C particles, and TiC_x spherules. The TiC_x layer is composed of coarsening TiC_x precipitates which are ejected into the progressively Ni-rich Ti-Ni melt. These TiC_x spherules vary in size with apparent diameters of approximately 0.2 to 1 μm. No distinct interface exists between the partially and fully reacted regions. Final consumption of C is followed by TiC_x spherule growth by combined Ostwald ripening and grain coalescence mechanisms resulting in an apparent diameter of 2.5 μm. The addition of Mo does not significantly affect the processes occurring within the partially reacted region. It is apparent that Mo enters into solution with the Ti-Ni melt at a rate much slower than that characteristic of the other processes (*i.e.*, Ti-Ni melt mixing or Ti-C reaction).

I. INTRODUCTION

THE synthesis of ceramics, intermetallics, and composites by combustion synthesis has been the subject of a considerable amount of recent research; this has encompassed both macrokinetics and micromechanisms.[1–22] The combustion synthesis in the Ti-C-Ni system has been studied by the combustion-wave arresting technique,[19,20] synchrotron X-ray radiation,[11] and thermal analysis.[22] The objective of this investigation is the elucidation of the physical processes occurring in the propagation of stable combustion waves in Ti-C-Ni and Ti-C-Ni-Mo powder mixtures using the wave arresting technique developed by Rogachev *et al.*[19,20] The results of this first part will be presented in this article, while analysis and further discussion will be presented in the companion article.[23]

II. EXPERIMENTAL PROCEDURES

High-purity (>99 pct) powders of elemental Ti, C, Ni, and Mo were used in this investigation. The particle sizes for the Ti, C, Ni, and Mo were 44 μm (−325 mesh), 2 μm, 3 μm, and 2 to 4 μm, respectively. The Ti powder consisted of particles with an irregular shape, as well as agglomerates. Particle sizes range from approximately 5 to 100 μm. Because of their irregular morphology, particles larger than 44 μm are able to pass through the 325 mesh powder sieve. The C powders exhibit a flakelike morphology and form large agglomerates with sizes on the order of 50 μm. The Ni powders exhibit a "filament" morphology in which the powders agglomerate to form long chains. The Mo powders consist of agglomerated particles with a spheroidal morphology.

Three powder mixtures were used in this investigation corresponding to the final product compositions (weight percent): (1) 70TiC, 30Ni; (2) 66TiC, 30Ni, and 4Mo; and (3) 62TiC, 30Ni, and 8Mo. Powders were dry mixed in a ceramic grinding jar with grinding media (2:1) under an Ar atmosphere for approximately 24 hours. The powders were then removed from the ceramic grinding jar and placed within a vacuum oven for a minimum of 24 hours.

Combustion wave velocity and temperature measurements were conducted on the compositions listed previously, using cylindrical specimens 3 cm in height and diameter with green densities approximately 60 pct of the theoretical. Figure 1 is a schematic illustration of the experimental fixture used for the specimens and thermocouples. During combustion wave propagation, the specimens expand due to liquid formation and gas evolution. This expansion not only has a detrimental effect on the integrity of the thermocouples but also affects the combustion wave velocity and temperature. The fixture shown in Figure 1 eliminates this problem. Tungsten-rhenium thermocouples with bead diameters of approximately 500 μm were used. Two thermocouple wells (3 mm in diameter) approximately 6-mm deep and 1.25 cm apart were drilled into the sides of the specimens; they were backfilled with reactant powder

J.C. LaSALVIA, Postdoctoral Fellow, Institute for Mechanics and Materials, and M.A. MEYERS, Professor, Department of Applied Mechanics and Engineering Sciences, are with the University of California, San Diego, CA 92093. D.K. KIM, formerly Materials Research Scientist with the Department of Applied Mechanics and Engineering Sciences, University of California, is Professor of Materials Science with the Department of Ceramic Science and Engineering, Korea Advanced Institute of Science and Technology, Taejon 205-701, Korea. R.A. LIPSETT, formerly Undergraduate Research Associate with the Department of Applied Mechanics and Engineering Sciences, University of California, is Graduate Student, Dept. of Engineering, University of Southern California, Los Angeles, CA 90007.

Manuscript submitted October 24, 1994.

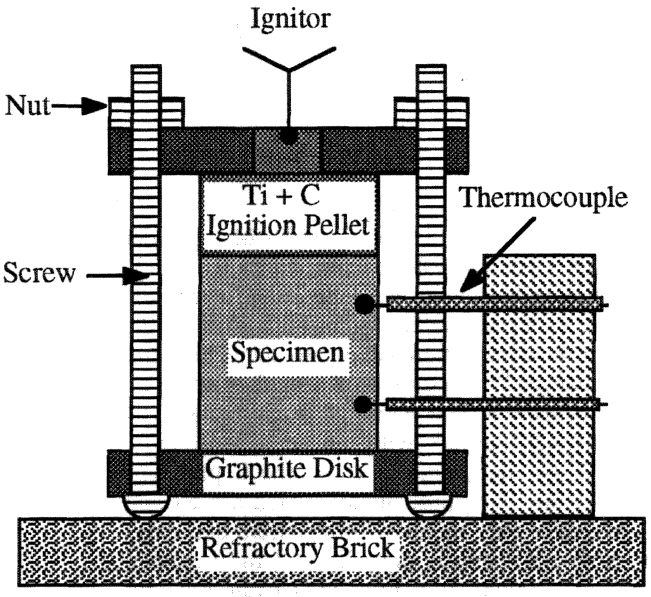

Fig. 1—Schematic illustration of the fixture used to constrain the longitudinal expansion of the specimen during combustion wave propagation.

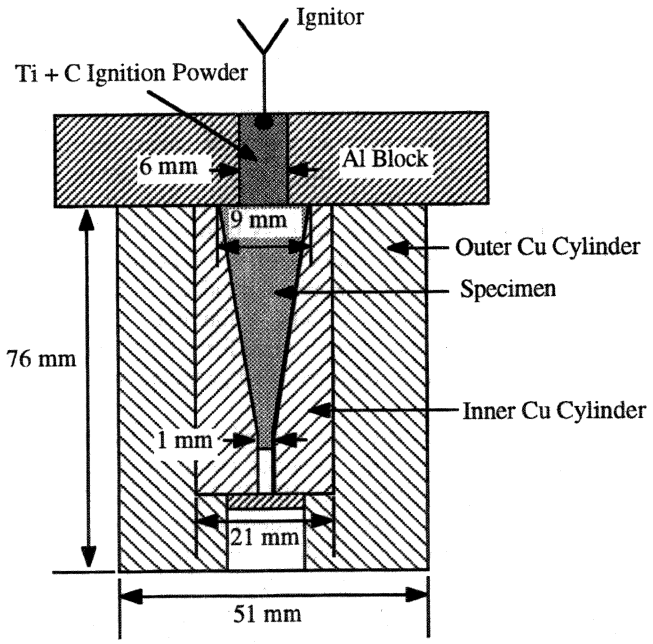

Fig. 2—Combustion-wave arresting experimental setup.

to improve contact between the thermocouple bead and the specimens. The thermocouples were held in position by an Al block (thermocouple wires were isolated from the block by a two-hole ceramic sleeve). Combustion wave propagation was initiated within the specimens indirectly by placing a 40 g Ti + C green compact (60 pct of theoretical green density) between the specimen and the ignition powder. This was done to ensure the uniform heating of the top surface of the specimen since this could not be guaranteed by using only the loose ignition powder. The ignition powder was initiated by a thermochemical match. Experiments were conducted in a controlled atmosphere (Ar) chamber.

The combustion-wave arresting technique used in this investigation is based on an approach developed by Rogachev *et al.*[19,20] It consists of a Cu cylinder with a conical hole in which the reactant mixtures are placed. The experimental setup is shown in Figure 2. It is placed within the test chamber under an Ar atmosphere to prevent oxidation of the specimen. The Cu cylinder consists of two main components: an outer Cu cylinder and an inner Cu cylinder which separates into two halves (for ease of specimen removal). An Al block is placed on top of the Cu cylinder to constrain the longitudinal expansion of the specimen during the reaction. As the cone radius decreases, the heat loss rate to the Cu cylinder per unit mass of reacted material increases. When it becomes of the same order as the characteristic time for the reaction, the reaction will not go to completion (at least for reactions with large activation energies). It is recognized that not all the physical processes occurring within the combustion wave can be effectively arrested or "quenched" using the Cu quench block technique because the cooling rate is not sufficiently high. Reactant powders are loaded into the Cu cylinder and lightly pressed to approximately 40 pct theoretical reactant density. The reaction is initiated using a thermochemical match and ignition powder. After each experiment, the specimen is infiltrated with epoxy, sectioned longitudinally, and polished using standard metallographic techniques. Specimens are carbon coated for observation by scanning electron microscopy (SEM).

III. RESULTS AND DISCUSSION

A. *Micromechanisms of Combustion Synthesis in the Ti-C-Ni System*

A numerical heat-transfer analysis was conducted on the experimental configuration shown in Figure 2, to estimate the cooling rates experienced during the quenching experiments. The specimen and Cu block were modeled as an inner solid cylinder and outer concentric cylinder, respectively. The effect of the taper on the cooling rate was determined by considering only radial heat conduction while varying the diameter of the specimen. Constant thermophysical properties were assumed and are listed in Table I.[24,25,26] The initial temperatures of the inner and outer cylinders were set at 2000 °C and 25 °C, respectively. Figure 3 shows the calculated temperature histories at various points on the axis of the cone. The simulation predicts that the temperature decreases from the maximum to room temperature in approximately 1 to 2 seconds. The maximum cooling rates vary from approximately 3×10^3 K/s (point 2) to 10^4 K/s (point 5). These cooling rates are of the same order as those obtained in the experimental studies of Mukasyan and Borovinskaya[16] and Merzhanov *et al.*[21] The variation in cooling rates is useful in "bracketing" the reaction.

In general, the macrostructure of the specimens consisted of a fully reacted region, a partially reacted region, and an unreacted region. These regions are shown in Figure 4 for the Ti + C + 30Ni reaction system and are marked 1, 2, and 3, respectively. No distinct interface exists between the fully reacted and partially reacted regions. This is due to the distribution in C agglomerate sizes. A distinct interface does exist between the partially reacted region and the unreacted region. This interface region is characterized by the formation of a Ni-Ti melt. Negligible interaction between

Table I. Thermophysical Properties Used in the Cooling Simulation Shown in Figure 3

Thermophysical Property	Cu[24]	Ni[24]	TiC[25,26]	TiC-Ni (40 Pct dense)
ρ (kg/m^3)	8930 at 293 K	8900 at 293 K	4930 at 293 K	—
k (W/mK)	398 at 293 K	83 at 373 K	17 at 293 K	—
C_p (J/kgK)	386 at 293 K	456 at 293 K	560 at 293 K	—
α (m^2/s)	1.1546×10^{-4}	2.0451×10^{-5}	6.1576×10^{-6}	3.6065×10^{-6}

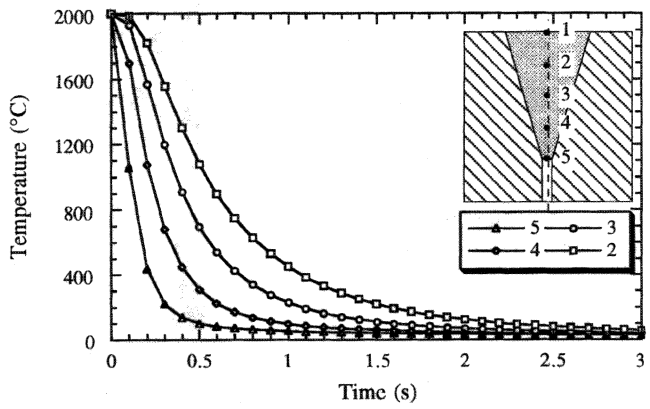

Fig. 3—Predicted temperature profiles for Cu block used in combustion-wave arresting experiments.

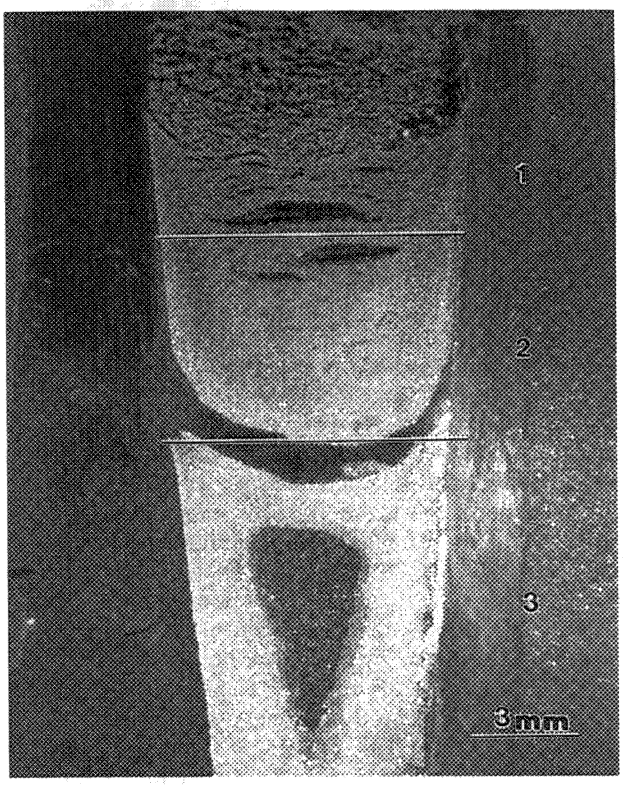

Fig. 4—Macroscopic view of a cross section of Ti-C-Ni specimen after reaction.

components is observed within the unreacted region, being limited only to contact regions. These three regions are described separately in Sections 1 through 3.

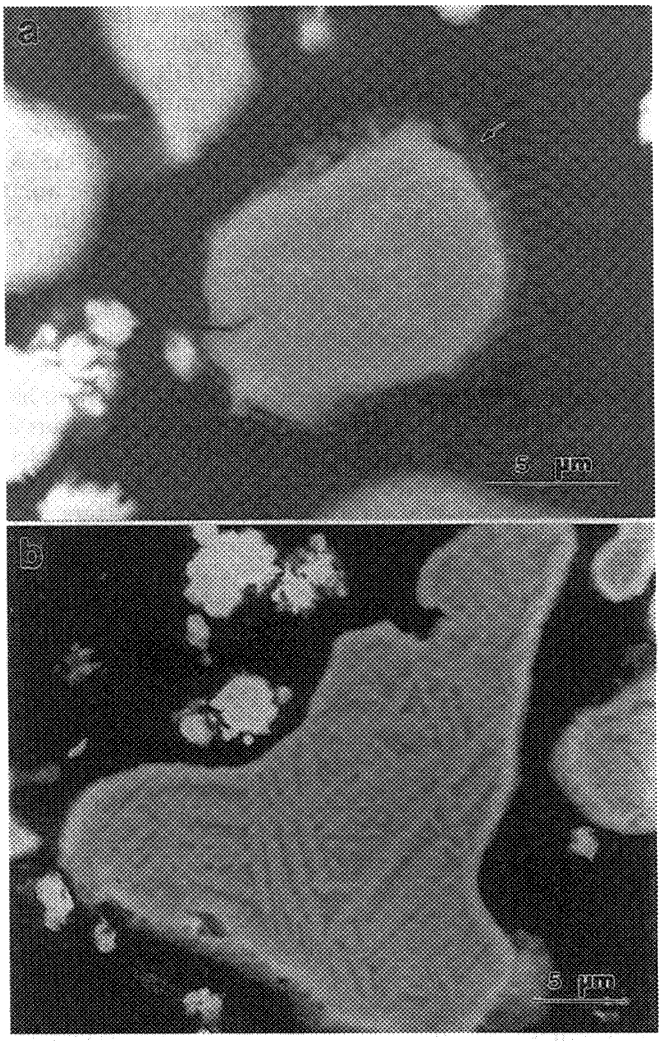

Fig. 5—(*a*) Reaction at the surface of a Ti particle, and (*b*) platelet features within a Ti particle indicating that it initially underwent the $\alpha \rightarrow \beta$ phase transformation.

1. *Unreacted region*

The first process observed to occur within the unreacted region is a reaction at the surface of the Ti particles, as shown in Figure 5(a). The uniformity of the reaction around the particles indicates that the reaction must be proceeding *via* the gas phase. Two possible explanations for the surface reaction may be either the dissolution of an oxide scale or decomposition of a hydride scale. Impurity analysis by the Ti powder manufacturer indicates that both H_2 (0.04 wt pct) and O_2 (0.08 wt pct) impurities are mainly contained at the surface of the Ti particles.[27] The results of Bloshenko *et al.*[28,29,30] suggest that if the O_2 content dissolved in the Ti

particles is below the solubility limit (increases with temperature), then the residence time of the Ti particles in the heat-affected (*i.e.*, unreacted) region is sufficiently long to dissolve an oxide scale thicker than 0.2 μm.[30] Assuming that the Ti particles are spherical and that all of the O_2 is bound within a TiO_2 scale, the thickness of the oxide scale would be approximately 16 nm and would be difficult to observe by SEM. The other possibility to consider is the decomposition of a hydride scale. TiH_2 decomposes at approximately 400 °C into Ti and H_2 at atmospheric pressure.[31] These temperatures are easily reached within the heat-affected region of the combustion wave. In studies of volatile impurity emissions during the combustion synthesis of TiC by Kecskes and Niiler[32] and of TiB_2 by Filonenko and Vershinnikov,[33] H_2 was one of the major gaseous impurities emitted during the reactions. Replacing O with H and using the same assumptions used to determine the oxide scale thickness, the thickness of the hydride scale would be approximately 85 nm. This correlates well with the observed thickness of the surface reaction. Furthermore, O_2 appears in combustion synthesized TiC (bound in as titanium oxycarbide)[28,29,30] and H_2 does not; this lends further support to the hypothesis that the surface reaction is the decomposition of TiH_2.

Figure 5(b) shows a Ti particle with evidence that it has undergone the α (hcp) $\rightarrow$ β (bcc) (transformation occurs at approximately 893 °C). The structure is either α platelets separated by the β phase (Widmanstätten structure) or α' platelets separated by the β phase.[34] This structure indicates that the Ti particle was subjected to a thermal cycle in which it was heated to a sufficiently high temperature such that it underwent the $\alpha \rightarrow \beta$ transformation. Note the sharpness of the particle surface, as well as the absence of the surface reaction. Thus, the scale has been completely removed before the melting of the particles.

2. *Partially reacted region*

The onset of the partially reacted region is generally characterized by the interaction of Ni with the Ti particles. As would be expected, the initial reaction between the Ni and Ti particles occurs at regions of contact and results in the formation of Ti-Ni compounds. Wong *et al.*[11] and Henshaw *et al.*[35] showed that Ti-Ni (TiNi or $TiNi_3$) compounds do form during combustion synthesis in the Ti-C-Ni system. Henshaw *et al.*[35] observed the propagation of two distinct combustion waves; the first appeared to be weakly exothermic (low brightness intensity), while the second was highly exothermic (high brightness intensity). X-ray diffraction spectroscopy after the first wave revealed reactant peaks, as well as peaks which indicated the presence of TiNi and Ti_2Ni.

Due to the exothermicity of the Ti-Ni reaction, a localized Ni-Ti melt forms which subsequently spreads over the surface of the Ti particles. Figure 6(a) is a close-up of the Ni-Ti reaction. With regard to this spreading, Korchagin and Aleksandrov[12] investigated the *in situ* reaction between Ti and C by electron microscopy and found that the spreading of the Ti melt over C is characterized by the simultaneous formation of TiC_x on the C surface. Thus, the Ti melt does not spread over the C surface but over a TiC_x layer. This indicates that the characteristic time for the formation of the layer is less than that for spreading. Spreading of a melt over the surface of a solid is related to its degree

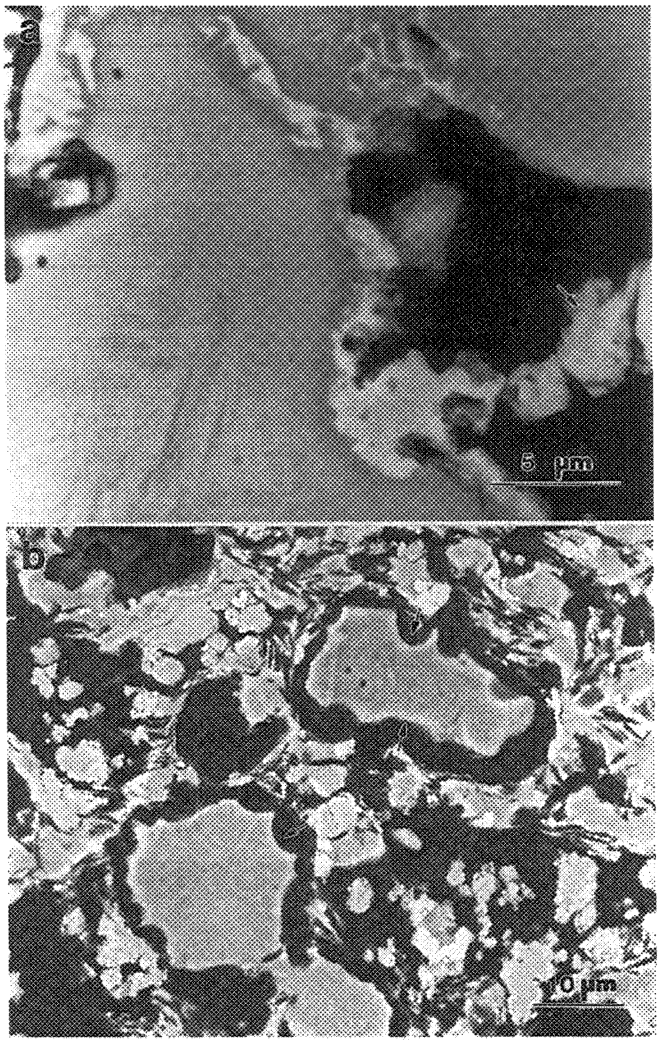

Fig. 6—(*a*) Interaction between Ni and Ti at contact region (initial Ti-Ni melt formation), and (*b*) nonuniform consumption of Ti particles due to interaction with Ni particles.

of wetting on the solid, as well as interfacial reactions.[36] According to Merzhanov *et al.*,[21] the spreading force F_s is given by the difference between the energies of adhesion W_A and of cohesion W_C (neglecting potential and kinetic energies). The energy of adhesion is the sum of the energies of intermolecular interaction (*e.g.*, adsorption) W_A^M and chemical bond formation W_A^B. The energy of cohesion is taken to be twice the liquid-gas interfacial energy γ_{lg}. Therefore, $F_s = W_A^M + W_A^B - 2\gamma_{lg}$. Note that for good wetting systems, γ_{lg} is smaller than for poor wetting systems.[37] The condition for spreading is that the spreading force F_s be greater than zero. Typically, for liquid metals, $W_C \approx 10^3$ mJ/m^2 while $W_A^M \approx 10^2$ mJ/m^2.[21] Consequently, the spreading of liquid metals on C is strongly dependent on chemical interaction. For the Ti-C system, $W_A^B \approx 10^3$ mJ/m^2.[21] For this reason, melt spreading and product formation are inseparable processes.

The Ni particle in Figure 6(a) (shown by arrow) indicates that the local temperature is below the melting point for Ni. The smaller Ti particles are consumed first through their interaction with Ni, while the larger particles are progressively consumed as one moves across the interface region, initially by the interaction with Ni and then by melting.

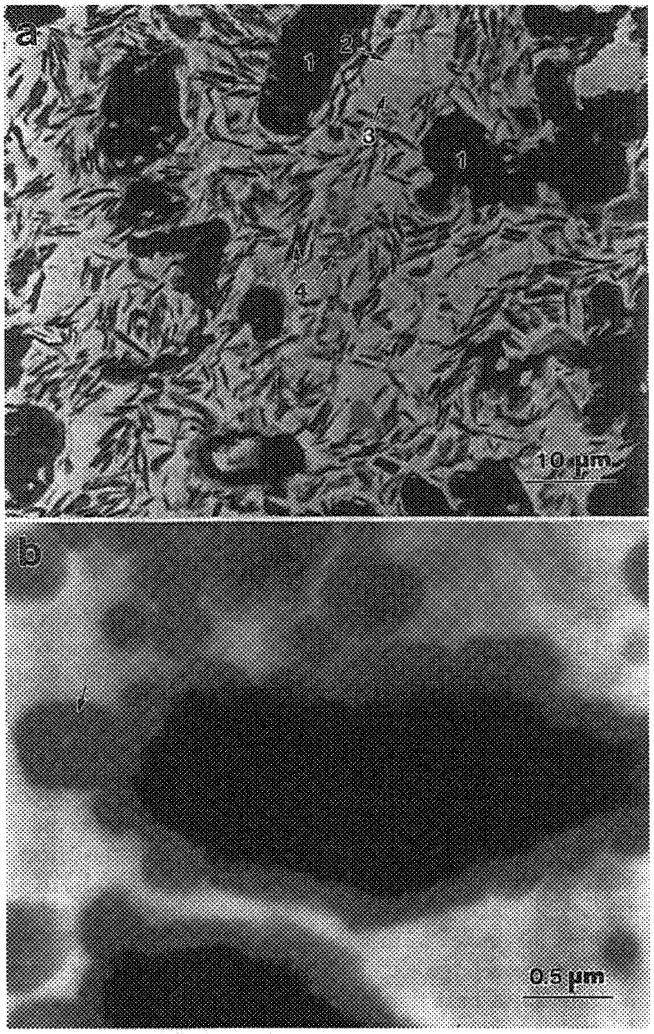

Fig. 7—(*a*) Partially reacted region showing porosity (1), Ti-Ni melt formation (2 and 3), and C (graphite) flakes (4); and (*b*) TiC_x layer covering the C particles.

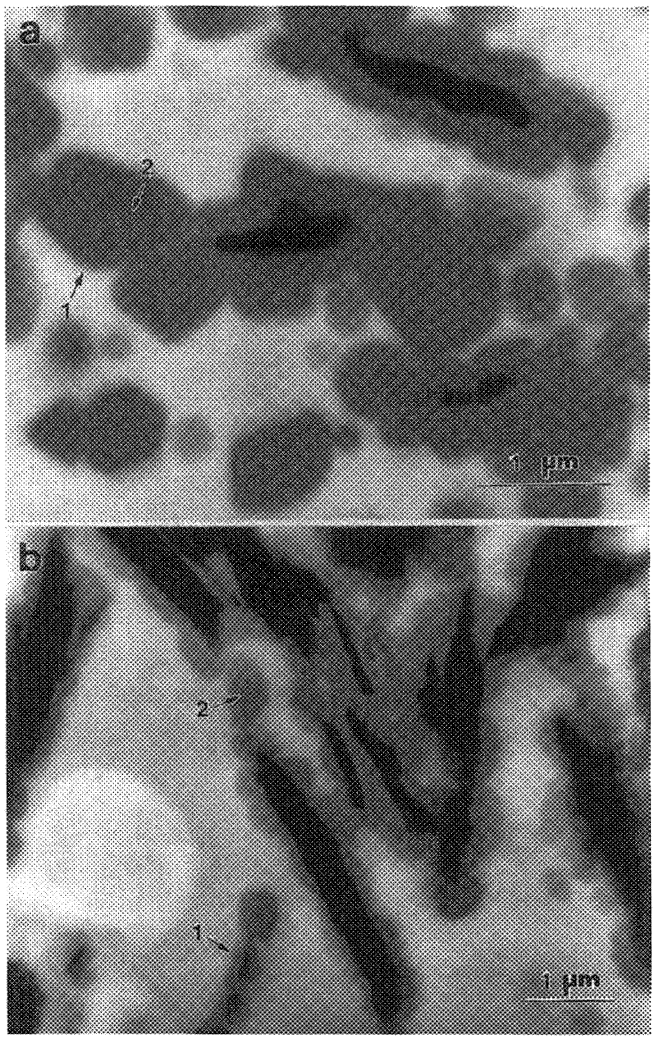

Fig. 8—(*a*) Formation of TiC_x spherules and separation of a TiC_x spherule from the edge of a C particle, and (*b*) formation of a rosary structure due to consumption of a C particle by growing TiC_x precipitates.

Because the reaction occurs first at contact regions, the consumption of the Ti particles is not uniform, as shown in Figure 6(b). Arrows indicate regions where localized interaction with Ni has taken place.

After the Ti particles have been completely consumed, the resulting Ti-Ni melt is initially inhomogeneous. This is a natural consequence of the fact that the powder mixture is heterogeneous and that there is a finite time required for intermixing between components once the melt has formed. This is shown in Figure 7(a). The large darker regions (1) are voids which formed due to the melting of the Ti particles followed by capillary flow.[38,39] Within the solidified Ti-Ni melt, light and dark regions are evident. The light regions (2) are Ni rich, while the dark regions (3) are Ni poor. Energy dispersive X-ray analysis of the light and dark regions yielded Ni weight percents of approximately 52 and 35 pct, respectively. As the temperature increases, the characteristic time for mixing decreases. The characteristic time for mixing or homogenization, assuming negligible times for either dissolution or melting, is given by $\tau_{mix} \approx \delta^2/D_{eff}(T)$, where δ is the average distance between the more refractory metal particles and D_{eff} is the effective diffusivity for these metal atoms within the melt, which is exponentially dependent on the temperature. The turbulent mixing due to temperature differences (*i.e.*, convective mixing) reduces the mixing length scale δ. The dark lenticular features (4) within the solidified Ti-Ni melt are C particles. Figure 7(b) shows that the C particles are covered with a TiC_x layer. The homogeneous distribution of the C particles within the solidified Ti-Ni melt, as shown in Figure 7(a), indicates that the Ti-Ni melt at least partially wets the TiC_x layer formed on the C particles. Solid-liquid systems in which the contact angle is less than 90 deg (*i.e.*, partial wetting conditions) are characterized by an equilibrium spacing of solid particles in the liquid, which depends upon the contact angle, particle size, and volume of liquid.[36]

As the temperature increases, the thickness of the TiC_x layer also increases. Eventually, for sufficiently large C particles, the TiC_x layer breaks up and "ejects" TiC_x spherules into the Ti-Ni melt. The apparent diameter of these spherules appears to be between 0.2 and 1 μm and is independent of the reactant particle sizes. Examination reveals that the formation of these spherules occurs first at the edges of the C particles (arrow in Figure 7(b)). Figure 8(a) shows TiC_x spherule which has separated from the TiC_x layer (shown by arrow 1). The breakup of the TiC_x layer en-

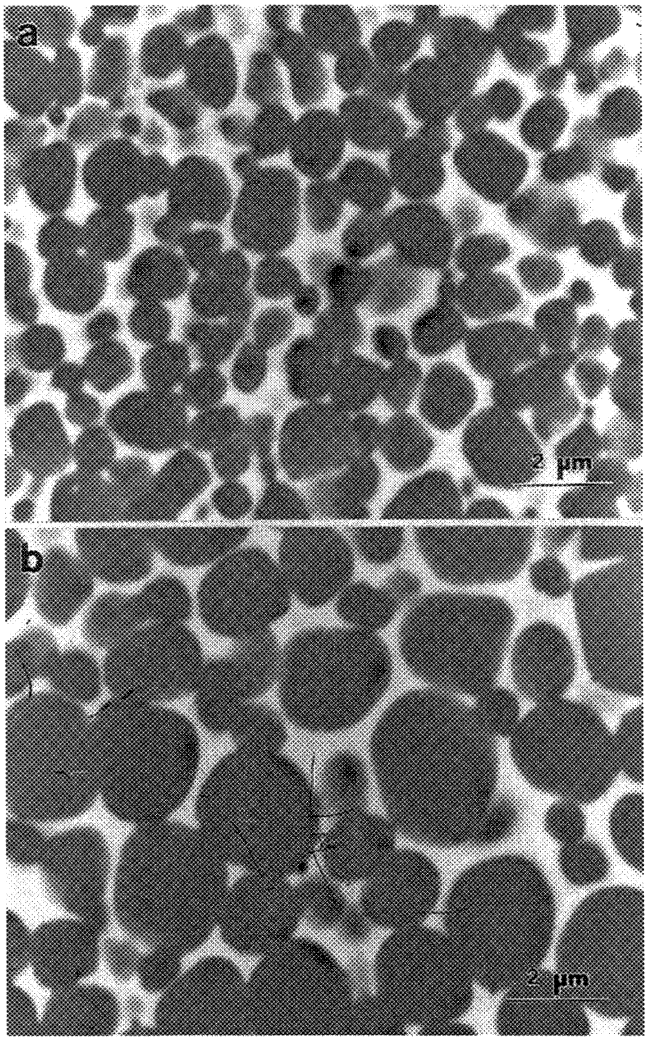

Fig. 9—Coarsening of TiC_x spherules in the fully reacted region with apparent diameters: (*a*) 1 μm and (*b*) 2.5 μm.

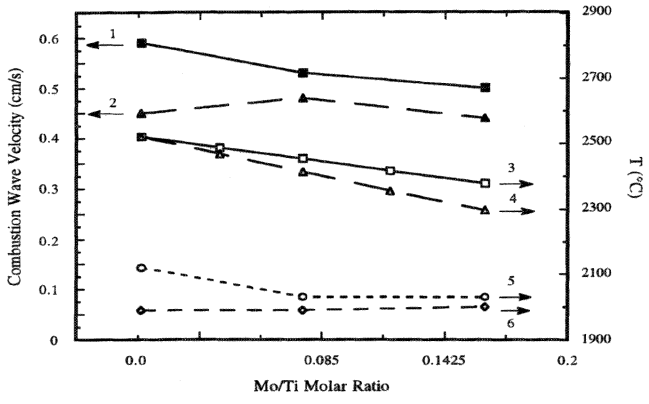

Fig. 10—Combustion wave velocity (U) and temperature (T_r) as a function of Mo/Ti molar ratio: (1) U, constrained end conditions; (2) U, unconstrained end conditions; (3) T_{ad}, Eq. [1]; (4) T_{ad}, Eq. [2]; (5) T_r, constrained end conditions; and (6) T_r, unconstrained end conditions.

hances the reaction rate by decreasing bulk diffusion distances. Final consumption of the C particles results in the formation of a "rosary" structure (arrow 1 in Figure 8(b)) which subsequently separates into individual TiC_x spherules. Residual C within some of the TiC_x spherules can be seen in Figures 8(a) and (b), as indicated by arrow 2.

3. *Fully reacted region*

After the C particles have been completely consumed, the TiC_x spherules undergo a process of rapid growth by dissolution reprecipitation (Ostwald ripening) and grain coalescence. The driving force for these processes is the minimization of the overall interfacial energy per unit volume (inversely proportional to the spherule diameter). This process is shown in Figures 9(a) and (b). The apparent diameter of the TiC_x spherules in Figure 9(a) is approximately 1 μm, while that in Figure 9(b) is 2.5 μm. This indicates that the maximum temperature and cooling rate are extremely important parameters in controlling the final spherule sizes for these materials. Dynamically densified specimens exhibited mean apparent spherule sizes of approximately 4 μm.[40]

B. *Effect of Mo Addition on the Ti-C-Ni Reaction*

The results of the combustion wave velocity (curves 1 and 2) and temperature measurements (curves 5 and 6) are shown in Figure 10 as a function of Mo/Ti molar ratio. Note that constraint has little effect on the combustion wave velocities. The most noticeable difference was in the reaction propagation mode. A stable macroscopically planar combustion wave was observed for constrained specimens, while two simultaneous "spin" waves were observed for the unconstrained specimens. Investigations on the effect of constraint in the combustion synthesis of TiC and TiB_2 by LaSalvia[41] and Kottke *et al.*,[42] respectively, revealed a 300 pct difference in the resulting velocities. Both TiC and TiB_2 undergo large expansions (>100 pct) which result in a decrease of heat flux into the unreacted region. Because Ni melts, is not a strong carbide former, and partially wets the resulting carbide phase, it counteracts the forces which cause swelling (*e.g.*, expansion of superheated gas trapped in isolated pores) with attractive capillary forces. As can be seen, the combustion wave velocity decreases with increasing Mo content for the constrained case (curve 1). Molybdenum is a weaker carbide former than Ti, and as a consequence, the exothermicity of the reaction decreases with increasing Mo/Ti molar ratio. This is reflected in the adiabatic temperatures for the reactions (curves 3 and 4). The adiabatic temperatures were calculated based upon the reaction equations

$$\mathrm{Ti + C + }y\mathrm{Ni + }z\mathrm{Mo \text{---}> TiC + }y\mathrm{Ni + }z\mathrm{Mo} \quad [1]$$

$$\mathrm{Ti + C + }y\mathrm{Ni + }z\mathrm{Mo \text{---}> [}(1-z)\mathrm{Ti},z\mathrm{Mo]C + }y\mathrm{Ni}(z\mathrm{Ti}) \quad [2a]$$

$$\mathrm{Ti + C + }y\mathrm{Ni + }z\mathrm{Mo \text{---}> [}(1-xz)\mathrm{TiC + }z\mathrm{Mo\ C}_{1-x}\mathrm{ + }y\mathrm{Ni}(xz\mathrm{Ti}) \quad [2b]$$

Equation [1] assumes that both Ni and Mo are inert additives, while Eqs. [2a] and [2b] assume that Mo interacts with TiC. It is well known that the addition of Mo (up to 40 wt pct) to TiC results in the formation of (Ti,Mo)C complex carbide.[43] The Mo atoms replace Ti atoms on the Ti sublattice of TiC. To the authors' knowledge, no thermodynamic data exist for this complex carbide. It was therefore assumed that the enthalpy of formation for this complex carbide could be calculated from the enthalpies of

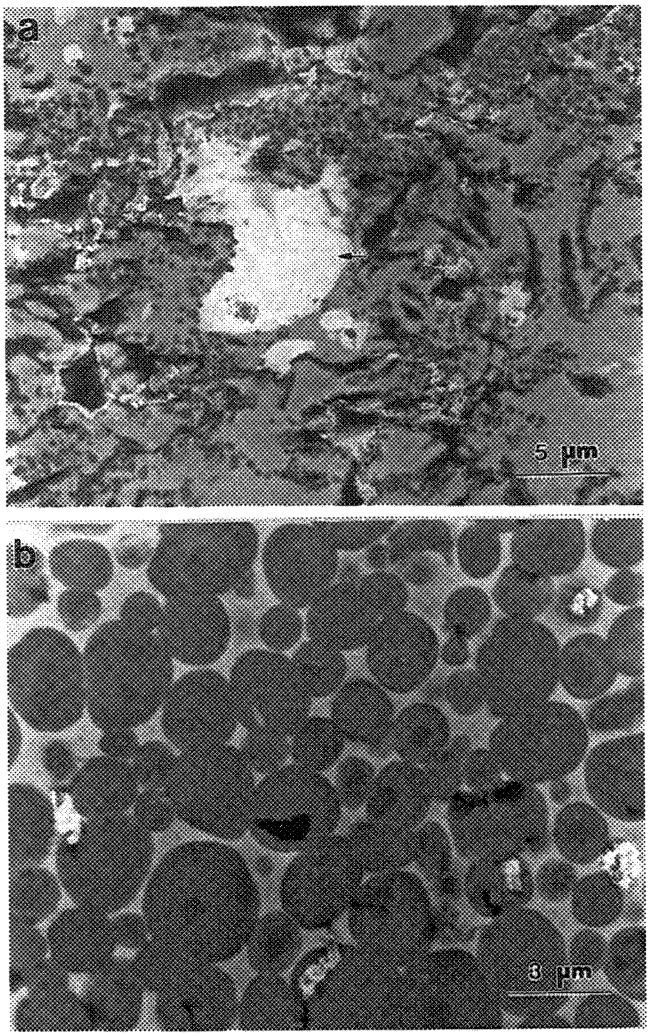

Fig. 11—(*a*) Large Mo agglomerate within partially reacted region; (*b*) final microstructure, coarsened carbide spherules with characteristic core/shell structure.

formation for TiC and Mo_2C ($x = 0.5$). The enthalpies of formation for TiC and Mo_2C are −184.1 and −49.5 kJ/mol, respectively.[44,45] The heat released in dissolving Ti into Ni was neglected in the adiabatic temperature calculation. From simple condensed phase combustion theory, the stable propagation velocity increases with increasing adiabatic temperature (or maximum combustion wave temperature).[46,47] Thus, it is expected that the combustion wave velocity will decrease with increasing Mo content. This is observed in Figure 10, curves 1 and 2. As will be seen, calculating the adiabatic temperature according to Eq. [1] may be more accurate than Eq. [2b], since Mo does not appear to affect the initial interaction between Ti and C. The experimentally measured maximum combustion wave temperatures are much lower than the adiabatic temperatures, as can be seen by comparing curves 3 through 6 in Figure 10. The exact reason for this discrepancy is not known.

Molybdenum does not affect many of the processes observed previously for several reasons: (1) the volume content of Mo is low; (2) the Mo particles form agglomerates; (3) Mo does not melt; and (4) Mo is a weak carbide former. Figure 11(a) shows a large Mo agglomerate (arrow) within the partially reacted region. As can be seen, TiC_x spherules have already formed. The Mo particle size was chosen to be small because its melting point (~2600 °C) is higher than the adiabatic temperatures of the reactions considered in this investigation and therefore would not be expected to melt during the reaction. It would have to enter the Ti-Ni-C melt by some other process (*e.g.*, reaction, dissolution, *etc.*). By whatever process Mo enters into solution with the melt, it is apparently slower than the initial interaction between Ti and C. Once in solution, Mo preferentially diffuses into the TiC_x spherules. Figure 11(b) shows the final microstructure. The core/shell structure within the carbide spherules is evident. The concentration of Mo is higher in the shell region of the carbide spherules.

IV. CONCLUSIONS

Table II summarizes the phenomena observed within the various regions of the combustion wave. Also shown is a schematic illustrating the approximate macroscopic temperature profile. The rectangular boxes indicate approximately the spatial occurrence of each process within the combustion wave. Overlapping of phenomena is the result of the initial heterogeneity of the reactant mixture (*i.e.*, chemical species, particle size, and particle size distribution). It is also noted that as a result of this initial heterogeneity, the microscopic temperature distribution within the plane of the combustion wave is not spatially uniform. The companion article[23] discusses the micromechanisms and kinetics in detail.

The unreacted region is characterized by both the breakdown of a scale on the Ti particles and the Ti $\alpha \rightarrow \beta$ solid-solid phase transformation. The scale either dissolves into the Ti particles if it is an oxide or decomposes if it is a hydride.

The partially reacted region is characterized by Ti-Ni melt formation and homogenization, capillary spreading, TiC_x formation, and TiC_x spherule formation. The apparent sizes of the TiC_x spherules appear to be independent of either the Ti or C reactant particle sizes. Mechanisms for the formation of these spherules are discussed in the companion article.[23]

The fully reacted region is characterized by TiC_x spherule coarsening and subsequent Ni melt crystallization. This indicates that the maximum temperature and cooling rate are extremely important parameters which can be controlled in order to optimize the final microstructure.

Molybdenum does not affect the main interaction between Ti and C, because the process by which it enters into solution with the Ti-Ni melt is apparently slower than the characteristic reaction time between Ti and C. It is this reaction which affects the combustion wave velocity because of its dominant exothermic nature. Once in the melt, Mo segregates itself to the TiC_x phase, resulting in the formation of the core/shell structure observed in conventionally processed materials.

ACKNOWLEDGMENTS

This research was supported by the United States Army Research Office under Contract Nos. ARO-DAAL-03-88-K-0194 and ARO-DAAL-03-90-G-0204 and by the Na-

Table II. Approximate Spatial Location of the Physical Processes Observed within the Arrested Combustion Wave

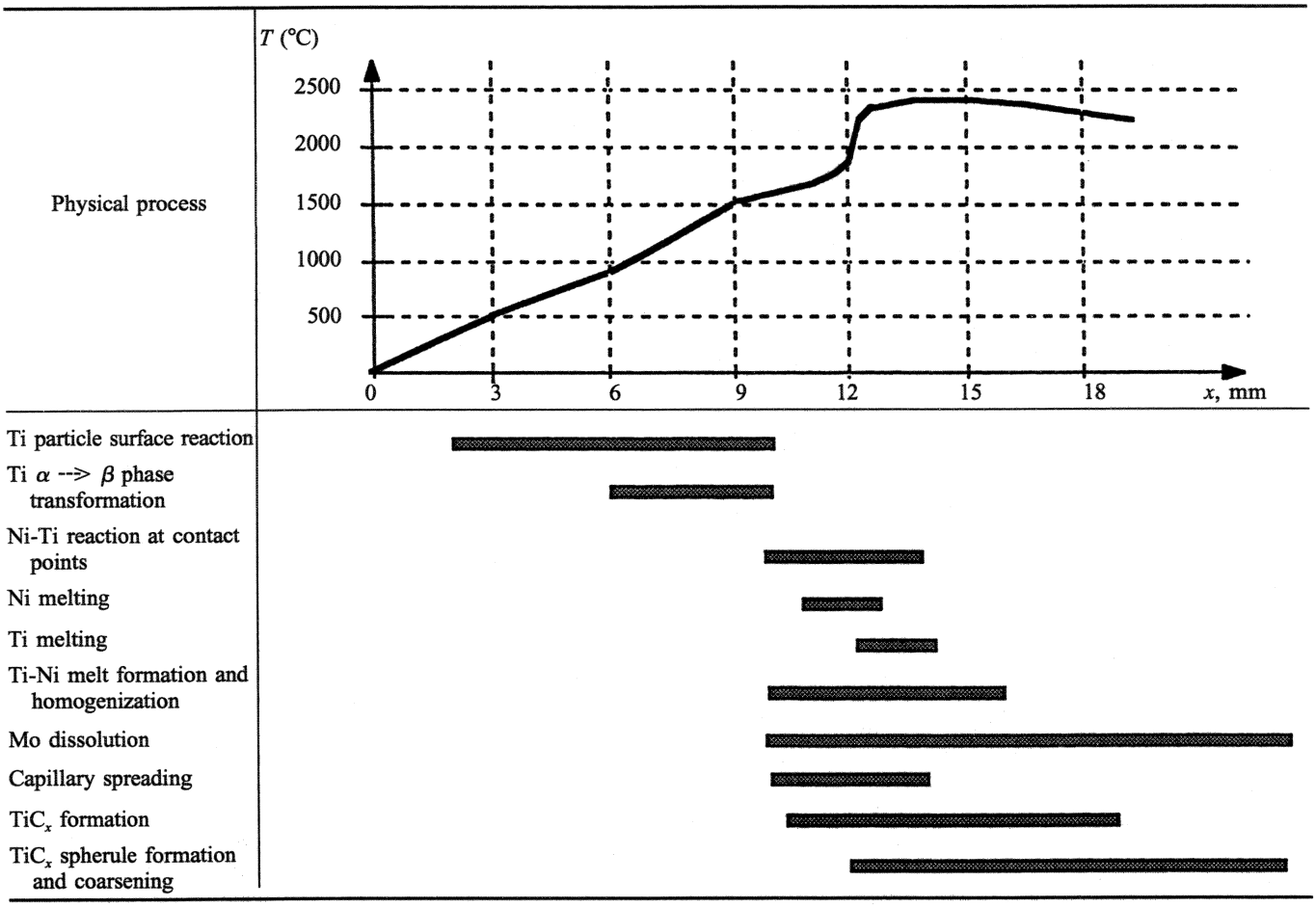

tional Science Foundation under Grant Nos. CBT-8713258, DMR-8713258, DMR-9116570, and DMR-9396132. We thank the continued support of Drs. E.S. Chen and A. Crowson. Support by the Institute for Mechanics and Materials, Dr. Richard Skalak, Director, is greatly appreciated. Discussions with Drs. A. Strutt and A. Niiler were very informative.

REFERENCES

1. Z.A. Munir and U. Anselmi-Tamburini: *Mater. hSci. Rep.*, 1989, vol. 3, pp. 277-365.
2. H.C. Yi and J.J. Moore: *J. Mater. Sci.*, 1990, vol. 25, pp. 1159-68.
3. A.G. Merzhanov: in *Combustion and Plasma Synthesis of High Temperature Materials*, Z.A. Munir and J.B. Holt, eds., VCH Publishers, New York, NY, 1990, pp. 1-53.
4. *J. Eng. Phys. Thermophys.*, 1993, vol. 63, pp. 1057-1170.
5. A.A. Zenin, A.G. Merzhanov, and G.A. Nersisyan: *Comb. Expl. Shock Waves*, 1981, vol. 17, pp. 63-71.
6. T. Boddington, P.G. Laye, J. Tipping, and D. Whalley: *Comb. Flame*, 1986, vol. 63, pp. 359-68.
7. S.D. Dunmead, Z.A. Munir, and J.B. Holt: *J. Am. Ceram. Soc.*, 1992, vol. 75, pp. 180-88.
8. E.A. Levashov, Yu. V. Bogatov, and A.A. Milovidov: *Combust. Explos. Shock Waves*, 1991, vol. 27, pp. 83-88.
9. S.C. Deevi: *J. Mater. Sci.*, 1991, vol. 26, pp. 2662-70.
10. V.V. Aleksandrov, M.A. Korchagin, B.P. Tolochko, and M.A. Sheromov: *Comb. Expl. Shock Waves*, 1984, vol. 19, pp. 430-31.
11. J. Wong, E.M. Larson, J.B. Holt, P.A. Waide, B. Rupp, and R. Frahm: *Science*, 1990, vol. 249, pp. 1406-09.
12. M.A. Korchagin and V.V. Aleksandrov: *Comb. Expl. Shock Waves*, 1981, vol. 17, pp. 58-63.
13. V.A. Shugaev, A.S. Rogachev, and V.I. Ponomarev: *Int. J. SHS*, 1992, vol. 1, pp. 72-77.
14. V.V. Aleksandrov and M.A. Korchagin: *Comb. Expl. Shock Waves*, 1987, vol. 23, pp. 557-64.
15. B.M. Vol'ne and V.V. Evstigneev: *Comb. Expl. Shock Waves*, 1992, vol. 28, pp. 173-78.
16. A.S. Mukasyan and I.P. Borovinskaya: *Int. J. SHS*, 1992, vol. 1, pp. 55-63.
17. A.G. Merzhanov and A.S. Rogachev: *Pure Appl. Chem.*, 1992, vol. 64, pp. 941-53.
18. V.M. Shkiro, V.N. Doroshin, and I.P. Borovinskaya: *Comb. Expl. Shock Waves*, 1980, vol. 16, pp. 370-74.
19. A.S. Rogachev, A.S. Mukas'yan, and A.G. Merzhanov: *Dokl. Akad. Nauk SSSR*, 1987, vol. 297, pp. 1240-43.
20. A.S. Rogachev, V.M. Shkiro, I.D. Chausskaya, and M.V. Shvetsov: *Comb. Expl. Shock Waves*, 1988, vol. 24, pp. 720-26.
21. A.G. Merzhanov, A.S. Rogachev, A.S. Mukas'yan, and B.M. Khusid: *Comb. Expl. Shock Waves*, 1990, vol. 26, pp. 92-102.
22. S.D. Dunmead, D.W. Readey, C.E. Semler, and J.B. Holt: *J. Am. Ceram. Soc.*, 1989, vol. 72, pp. 2318-24.
23. J.C. LaSalvia and M.A. Meyers: *Metall. Mater. Trans. A*, 1995, vol. 26A, pp. 0000-00.
24. P. Schwarzhopf, R. Kieffer, W. Leszynski, and F. Benesovsky: *Refractory Hard Metals*, MacMillan Company, New York, NY, 1953.
25. E.K. Storms: *The Refractory Carbides*, Academic Press, New York, NY, 1967.
26. *Metals Handbook*, 10th ed., vol. 2, *Properties and Selection: Nonferrous Alloys and Special-Purpose Materials*, ASM INTERNATIONAL, Metals Park, OH, 1990.
27. Micron Metals Inc., Salt Lake City, UT.
28. V.N. Bloshenko, V.A. Bokii, and I.P. Borovinskaya: *Comb. Expl. Shock Waves*, 1984, vol. 20, pp. 673-75.
29. V.N. Bloshenko, V.A. Bokii, I.P. Borovinskaya, and A.G. Merzhanov: *Comb. Expl. Shock Waves*, 1984, vol. 20, pp. 676-80.

30. V.N. Bloshenko, V.A. Bokii, and I.P. Borovinskaya: *Comb. Expl. Shock Waves*, 1985, vol. 21, pp. 88-92.
31. *Metal Hydrides*, W.M. Mueller, J.P. Blackledge, and G.G. Libowitz, eds., Academic Press, New York, NY, 1968, pp. 338-46.
32. L.J. Kecskes and A. Niiler: *J. Am. Ceram. Soc.*, 1989, vol. 72, pp. 655-61.
33. A.K. Filonenko and V.I. Vershinnikov: *Sov. J. Chem. Phys.*, 1985, vol. 3, pp. 675-82.
34. *Titanium and Titanium Alloys*, M.J. Donachie, Jr., ed., ASM, Metals Park, OH, 1982.
35. W.F. Henshaw, A. Niiler, and T. Leete: Report No. ARBRL-MR-03354, Aberdeen Proving Ground, MD, Apr. 1984.
36. R.M. German: *Liquid Phase Sintering*, Plenum Press, New York, NY, 1985.
37. *Cermets*, J.R. Tinklepaugh and W.B. Crandall, eds., Reinhold, New York, NY, 1960.
38. V.M. Shkiro and I.P. Borovinskaya: *Comb. Expl. Shock Waves*, 1976, vol. 12, pp. 828-31.
39. A.I. Kirdyashkin, Yu. M. Maksimov, and A.G. Merzhanov: *Comb. Expl. Shock Waves*, 1981, vol. 17, pp. 591-95.
40. J.C. LaSalvia, M.A. Meyers, and D.K. Kim: *J. Mater. Synthesis and Processing*, 1994, vol. 2, pp. 255-74.
41. J.C. LaSalvia: Ph.D. Dissertation, University of California, San Diego, CA, 1994.
42. T. Kottke, L.J. Kecskes, and A. Niiler: Ballistic Research Laboratory Memorandum Reports BRL-MR-3793 and BRL-MR-3574, Aberdeen Proving Ground, MD, Dec. 1989.
43. V.N. Eremenko, T. Ya. Velikanova, and S.V. Shabanova: in *Refractory Carbides*, G.V. Samsonov, ed., Consultants Bureau, New York, NY, 1974, pp. 143-55 (English translation).
44. M.W. Chase, Jr., C.A. Davies, J.R. Downey Jr., D.J. Frurip, R.A. McDonald, and A.N. Syverud: *JANAF Thermochemical Tables*, 3rd ed., part I, *Al-Co; J. Phys. Chem. Ref. Data*, 1985, vol. 14, suppl. 1, American Chemical Society and American Institute of Physics for the National Bureau of Standards, 1986.
45. *Thermochemical Properties of Inorganic Substances: II*, 2nd ed., O. Knacke, O. Kubaschewski, and K. Hesselman, eds., Springer-Verlag, New York, NY, 1991.
46. B.V. Novozhilov: *Dokl. Acad. Sci. USSR, Phys. Chem.*, 1961, vol. 141, pp. 836-38, (English translation).
47. E.I. Maksimov, A.G. Merzhanov, and V.M. Shkiro: *Combust. Explos. Shock Waves*, 1965, vol. 1, pp. 15-18.